Magnetic-field- and temperature-dependent Fermi surface of CeBiPt

New Journal of Physics
The open-access journal for physics

Magnetic-field- and temperature-dependent Fermi surface of CeBiPt

J Wosnitza[1,7], G Goll[2], A D Bianchi[1], B Bergk[1], N Kozlova[3], I Opahle[3], S Elgazzar[3,8], Manuel Richter[3], O Stockert[4], H v Löhneysen[2,5], T Yoshino[6] and T Takabatake[6]

[1] Hochfeld-Magnetlabor Dresden (HLD), Forschungszentrum Rossendorf, D-01314 Dresden, Germany
[2] Physikalisches Institut, Universität Karlsruhe, D-76128 Karlsruhe, Germany
[3] IFW Dresden, PO Box 270116, D-01171 Dresden, Germany
[4] Max-Planck-Institut für Chemische Physik fester Stoffe, D-01187 Dresden, Germany
[5] Forschungszentrum Karlsruhe, Institut für Festkörperphysik, D-76021 Karlsruhe, Germany
[6] Department of Quantum Matter, ADSM, Hiroshima University, Higashi-Hiroshima 739-8530, Japan
E-mail: J.Wosnitza@fz-rossendorf.de

New Journal of Physics **8** (2006) 174
Received 2 May 2006
Published 1 September 2006
Online at http://www.njp.org/
doi:10.1088/1367-2630/8/9/174

Abstract. The half-Heusler compounds CeBiPt and LaBiPt are semimetals with very low charge-carrier concentrations as evidenced by Shubnikov–de Haas (SdH) and Hall-effect measurements. Neutron-scattering results reveal a simple antiferromagnetic structure in CeBiPt below $T_N = 1.15$ K. The band structure of CeBiPt sensitively depends on temperature, magnetic field and stoichiometry. Above a certain, sample-dependent, threshold field ($B > 25$ T), the SdH signal disappears and the Hall coefficient reduces significantly. These effects are absent in the non-4f compound LaBiPt. Electronic-band-structure calculations can well explain the observed behaviour by a 4f-polarization-induced Fermi-surface modification.

[7] Author to whom any correspondence should be addressed.
[8] Also at: Department of Physics, Faculty of Science, Menoufia University, Shebin El-kom, Egypt.

PII: S1367-2630(06)23697-8

Contents

1. Introduction

The electronic band structure is known to be a rather robust property of the metallic state. In particular, external magnetic fields usually cannot modify the Fermi surface of metals. This is easily plausible from the different typical energy scales involved, which are in the eV range for the Fermi energy and some meV for the Zeeman energy even at the pulsed magnetic fields in the 50 T range applied here. Therefore, for an ordinary Fermi liquid in the paramagnetic metallic state changes of the Fermi-surface topology caused by external fields—also called Lifshitz transitions [1]—may be disregarded. Equally unusual is a noticeable modification of the Fermi-surface area with temperature.

Here, we report on electrical-transport measurements of CeBiPt which exactly reveal these unexpected features. Clear Fermi-surface changes can be observed as a function of temperature and magnetic field. The absence of any unusual field and temperature-dependent band-structure modifications in the homologous non-4f compound LaBiPt proves the Ce 4f electrons as the major cause for the peculiarities in the metallic state of CeBiPt. Although in both semimetals, the experimentally determined Fermi energies are comparably small (about 25 meV for CeBiPt), the conventional Zeeman energy (∼6 meV at 50 T) cannot account for the observations. Only by identifying the polarization of the 4f moments by the external magnetic field, band-structure calculations are able to disclose the Fermi-surface changes as a magnetic-field-induced Lifshitz transition [2]. Measurements of a sample with probably slightly different stoichiometry prove that the size of the observed effects sensitively depends on the exact density of states at the Fermi level.

The ternary intermetallic compounds RBiPt (R is a rare-earth metal) show a rich variety of ground-state properties, ranging from superconductivity (for R = La) over antiferromagnetic order (R = Ce) and small-gap semiconducting behaviour (R = Nd) to the super-heavy-fermion metal YbBiPt, that shows a linear specific-heat coefficient of 8 J mol^{-1} K^{-2} [3, 4]. The RBiPt compounds have the cubic MgAgAs crystal structure, also called half-Heusler structure (figure 1). The lattice constants reduce from 6.87 Å (for R = La) to 6.59 Å (Lu) in the series [3]. After some early ambiguities, neutron-diffraction experiments on YbBiPt [5] as well as total-energy calculations using relativistic band-structure calculations [6] have revealed that Pt resides at the (0, 0, 0) position, i.e. the only site having two neighbour atoms along the [1 1 1] direction because the (1/2, 1/2, 1/2) site is empty.

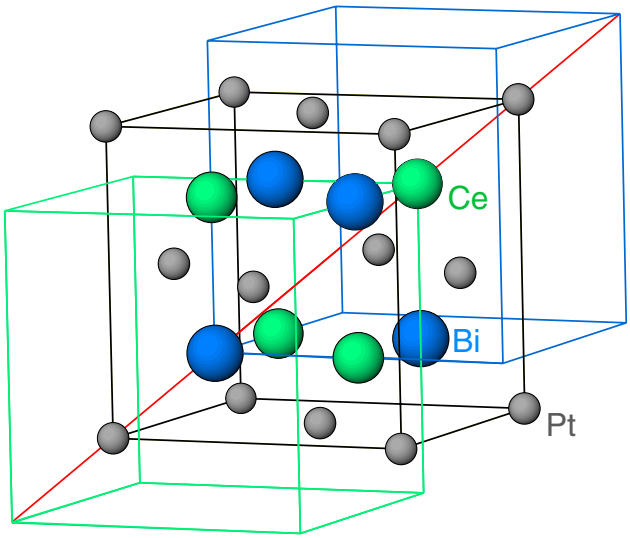

Figure 1. The half-Heusler crystal structure of CeBiPt which consists of three fcc sublattices for Pt, Bi and Ce, which are highlighted by different colours. The relative atomic coordinates are (0, 0, 0), (1/4, 1/4, 1/4) and (3/4, 3/4, 3/4), respectively.

2. Experimental

All investigated samples were prepared at Hiroshima University. The single crystals were grown by use of the Bridgman technique in hermetically sealed Mo crucibles from the starting materials Ce (m5N, Ames Laboratory), Bi (m5N), Pt (m3N) and La (m4N). To avoid oxidation of elemental Ce or La during handling, CePt or LaPt was first prepared by argon-arc melting and the appropriate amount of Bi was then added. For the CeBiPt crystals, an excess amount of about 40% Bi was added. The crucible, sealed under Ar atmosphere, was heated to 1350°C with an intermediate halt at 500°C for 2 h. After 12 h, it was slowly cooled by moving it out of the central zone of the furnace with 1 mm h^{-1}. Whether the 1-1-1 compounds or 3-4-3 compounds like $Ce_3Bi_4Pt_3$ are formed in the Bi flux depends very sensitively on the excess amount of Bi.

Neutron-diffraction experiments were performed on 9 g CeBiPt powder using the diffractometer E6 at the Hahn–Meitner-Institut (HMI), Berlin, with a neutron wavelength $\lambda = 2.444$ Å as well as on the diffractometer D23 at the ILL/Grenoble using a CeBiPt single crystal with dimensions of about $3 \times 3 \times 3\,\mathrm{mm}^3$ with a neutron wavelength $\lambda = 1.276$ Å in the temperature range $T = 30\,\mathrm{mK} - 2\,\mathrm{K}$.

The electrical-transport measurements were performed at the High Magnetic Field Laboratory at Dresden (HLD) in pulsed fields up to about 50 T. For the transport measurements up to six 40 μm gold wires were attached to the samples with graphite paste. The samples themselves were tightly glued to the sample holders with IMI7031 varnish. AC currents up to 1 mA with frequencies between 10 and 50 kHz were applied for about 80 ms just before and during the field pulse. The reliability of the data was checked for different currents and frequencies. The best signal-to-noise ratios were found on the falling side of the field pulses. In the following, only the data of these down sweeps are shown. Uncertainties of the geometry factors result in error bars of about 20% in the absolute resistivities. Since small misalignments of the contacts

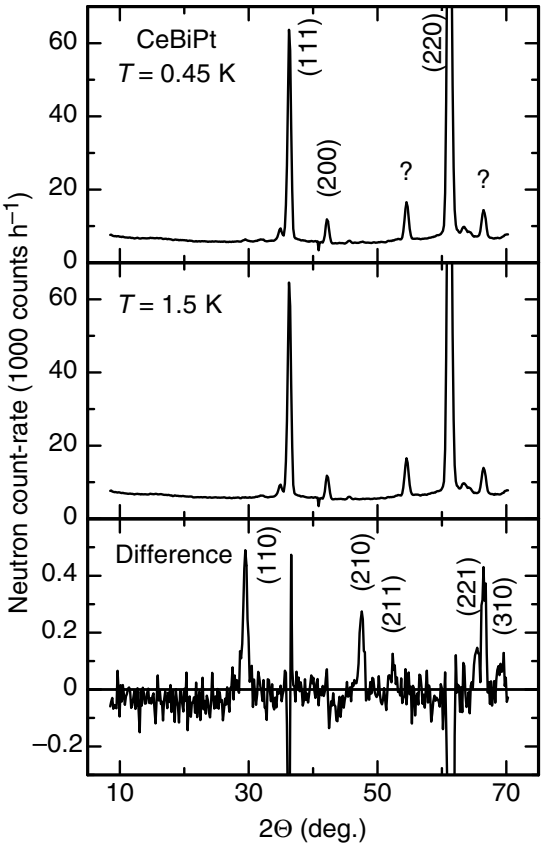

Figure 2. Neutron count rate versus scattering angle 2Θ in CeBiPt powder at the nominal temperature $T = 0.45$ K (top panel) and $T = 1.5$ K (middle panel). The bottom panel shows the difference diffraction pattern. The data were taken on E6 at HMI with $\lambda = 2.444$ Å.

are unavoidable, the longitudinal and transverse (Hall) resistances in most cases were extracted from positive and negative field pulses applied successively at each temperature. The overall agreement between the pulsed-field and earlier static-field data [2, 7] is excellent.

3. Results and discussion

3.1. Neutron scattering

As evidenced by specific-heat and magnetization measurements, our CeBiPt samples order antiferromagnetically at about 1.1 K [8]. This is somewhat at odds with an earlier report of an ordering temperature of 2.5 K [3]. In order to investigate the magnetic order closer, a neutron-diffraction experiment was performed on about 9 g CeBiPt powder at the HMI Berlin. Powder-diffraction patterns were recorded at several temperatures below and above $T_N = 1.15$ K. Figure 2 displays the diffraction pattern of CeBiPt up to $2\Theta = 70^\circ$ taken at 0.45 and 1.5 K together with the difference pattern. However, although helium was used as exchange gas in the sample container to improve the thermal coupling, the powder decoupled thermally below ≈0.6 K (see figure 3

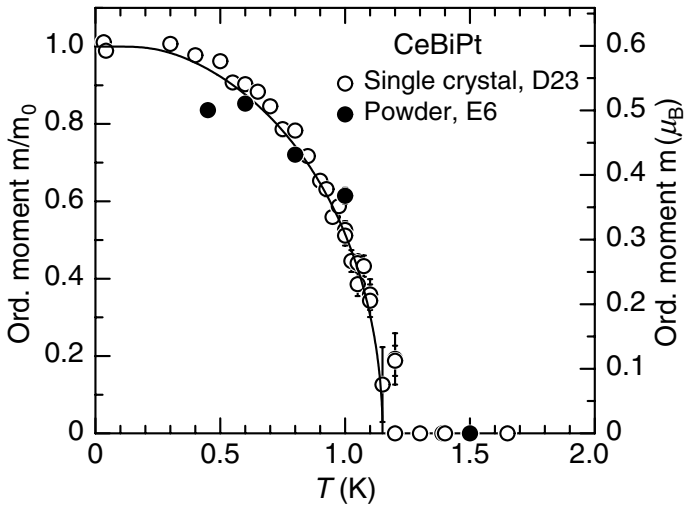

Figure 3. Temperature dependence of the ordered magnetic moment in CeBiPt as extracted from powder and single-crystal neutron-diffraction measurements (closed and open symbols, respectively). The solid line is a fit of a Brillouin function to the data.

(closed symbols)). No further increase in the ordered moment could be observed. In accordance with the mentioned thermodynamic measurements no magnetic intensity has been detected at 1.5 K. The crystal structure is confirmed to be cubic with a lattice constant $a = 6.793(4)$ Å at $T = 1.5$ K. Two nuclear peaks (marked by '?') originate from an impurity phase and do not belong to the CeBiPt structure. This impurity phase was observed only for the CeBiPt powder which seems to oxidize quite rapidly in air. It should be mentioned that no deterioration of the CeBiPt single crystals used for the electrical-transport measurements was observed over many years (see below). Magnetic intensity can hardly be seen directly in the powder-diffraction data taken at nominal $T = 0.45$ K. However, the difference pattern clearly shows magnetic peaks. They can be easily indexed and indicate that the antiferromagnetic structure is a type-I structure with a propagation vector $\tau = (1\,0\,0)$ and moments also along [1 0 0].

To study the temperature dependence of the antiferromagnetic order in detail, single-crystal neutron diffraction was carried out on the diffractometer D23 at the ILL/Grenoble. Since the magnetic (1 1 0) reflection was spoiled, due to a considerable amount of $\lambda/2$ contamination in the incident neutron beam on D23, the clearly resolvable magnetic (2 2 1) reflection was analysed instead. The results are plotted in figure 3 by open symbols. The Néel temperature was determined to $T_N = 1.15$ K in good agreement with the thermodynamic measurements [8]. The ordered moment m was extracted from the data via the relation $I \propto m^2$ where I denotes the magnetic intensity. However, a direct determination of the absolute value of the ordered moment from the single-crystal measurements was hampered by strong extinction effects due to the large crystal size and the high crystallographic symmetry. Therefore, these measurements only yield the normalized ordered moment m/m_0 which was scaled to match the powder measurements in the region of overlap. At lowest temperature, this analysis reveals an ordered magnetic moment $m_0 = 0.6\mu_B$ at the Ce site that is somewhat smaller than the value expected for the Γ_8 quartet ground state, the reason of which is not clear yet. Surprisingly, the entire temperature variation of the magnetic intensity is well described by a Brillouin function with $J = 5/2$ (solid line in

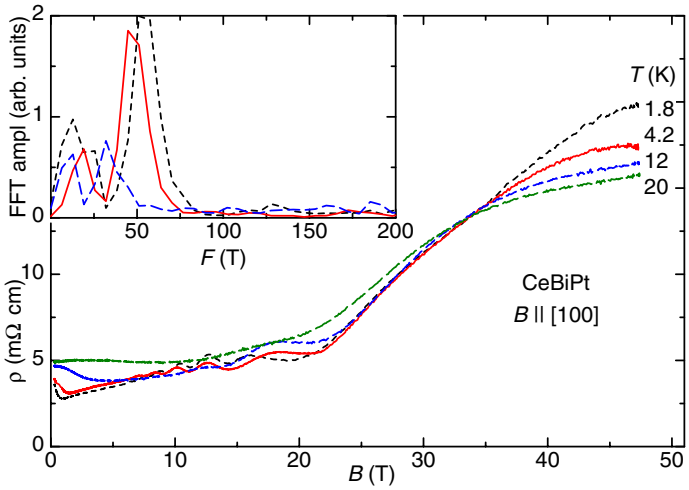

Figure 4. Field dependence of the resistivity ρ of CeBiPt for selected temperatures. The inset shows the corresponding Fourier spectra of the SdH signals.

figure 3) which is expected within a mean-field approach. Consequently, the neutron-scattering data indicate that around T_N, the usually expected critical fluctuations are weak for CeBiPt.

3.2. Electrical transport

The pulsed-field measurements of the longitudinal and transverse resistivities presented below were done well in the paramagnetic state at temperatures above T_N. Furthermore, as specific-heat data have shown, even at low temperatures antiferromagnetic order is suppressed completely at applied magnetic fields above 1.5 T [8].

Figure 4 shows the magnetoresistance of CeBiPt for selected temperatures between 1.8 and 20 K and with the magnetic field applied along [1 0 0]. The pulsed-field data agree very well with the static-field data measured some years earlier and reported previously [7]. The initial decrease of the resistivity, ρ, reflects most probably antiferromagnetic fluctuations above T_N in the paramagnetic state as evident from its absence at 20 K. This shows that, contrary to the small fluctuation effects observed by neutron scattering, the electronic transport is strongly influenced by these fluctuations at low magnetic fields and temperatures. Up to about 25 T, the well-known Shubnikov–de Haas (SdH) oscillations can be resolved at lower temperatures. The unusual effect here is, however, the temperature-dependent change of the SdH frequency, F, as has been observed for the static-field data as well [7]. As can be seen from the Fourier spectra shown in the inset of figure 4, F reduces from about 55 T at 1.8 K to 33 T at 12 K.

The anomalous T dependence of F is found only for field along the [1 0 0] and the equivalent [0 1 0] directions where F is found to be about 60 T for $T \to 0$ (figure 5(b)). As shown by SdH data obtained in static fields using a rotatable sample holder [7], F is constant at 30 T and furthermore independent of T between approximately $\Theta = 20^\circ$ and 70°, where Θ is the angle from the [1 0 0] direction toward [0 1 0] (figure 5(b)). For B along the [1 1 1] direction, a very low SdH frequency of about 20 T—but again independent of T—is found. The quantum-oscillation frequencies for the non-4f reference metal LaBiPt (see also figure 7 below) are independent of T for all angles and somewhat larger (65 T for B along [1 0 0] increasing to 95 T for B along [1 1 0])

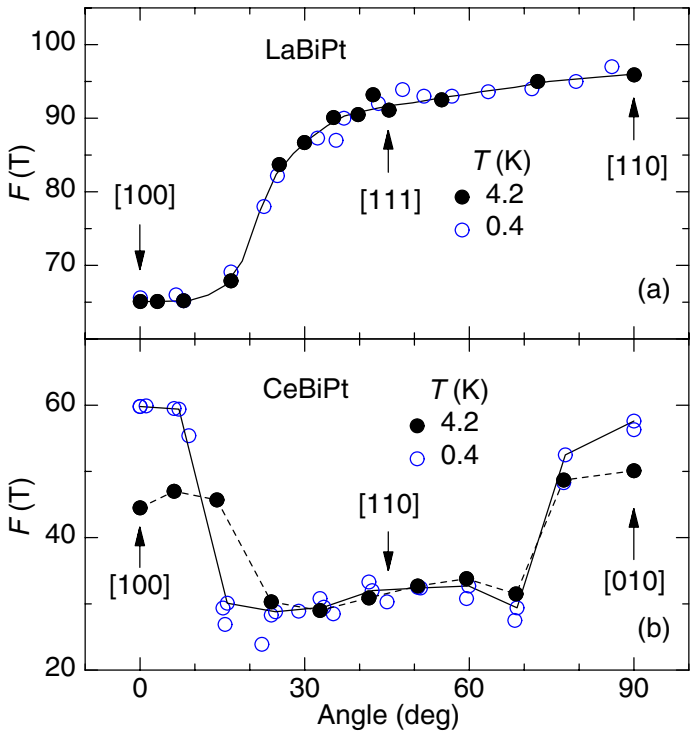

Figure 5. Angular dependences of the SdH frequencies of (a) LaBiPt and (b) CeBiPt for two different temperatures.

than for CeBiPt, as shown in figure 5(a). For both materials, the SdH signal can be followed over the whole angular range. This indicates simple singly connected Fermi surfaces, in line with band-structure calculations discussed below.

From the temperature dependence of the SdH-oscillation amplitudes, $A(T)$, the cyclotron effective masses, m_c, can be extracted. For CeBiPt, $A(T)$ for B along [1 0 0] was determined graphically by interpolating between the SdH-oscillation maxima. By use of the standard expression $A(T) \propto T/\sinh(\alpha(T/B)(m_c/m_e))$, with $\alpha = 2\pi^2 k_B m_0/e\hbar = 14.69\,\mathrm{T/K}$ [9], we obtain the effective mass $m_c = 0.24\,m_e$, where m_e is the free-electron mass. For $B \parallel$ [1 1 0] where F is independent of T, we find $m_c \approx 0.3\,m_e$. These low effective masses as well as specific-heat results, that only can give an upper limit for the electronic contribution (less than $25\,\mu\mathrm{J\,mol^{-1}\,K^{-2}}$) [8], clearly show that the Kondo effect giving rise to heavy-fermion behaviour in many other Ce-based metals obviously plays a negligible role for CeBiPt.

Besides the unusual temperature-dependent SdH frequency, another important observation is the vanishing of the oscillating signal above about 25 T and the prominent increase of the resistance above this field (figure 4). In another pulsed-field experiment, it was shown that the resistance increase can be followed up to 60 T and that the SdH oscillations vanish, independent of sample orientation in field [10]. This contrasts with the mentioned temperature-dependent change of the Fermi surface that occurs only for fields aligned within about 15° along the main cubic lattice vector.

Further information on this field-induced band-structure modification is obtained from a study where the longitudinal and the transverse resistances were measured simultaneously in pulsed fields [2]. As shown in figure 6, these measurements reproduced well the previous ρ data

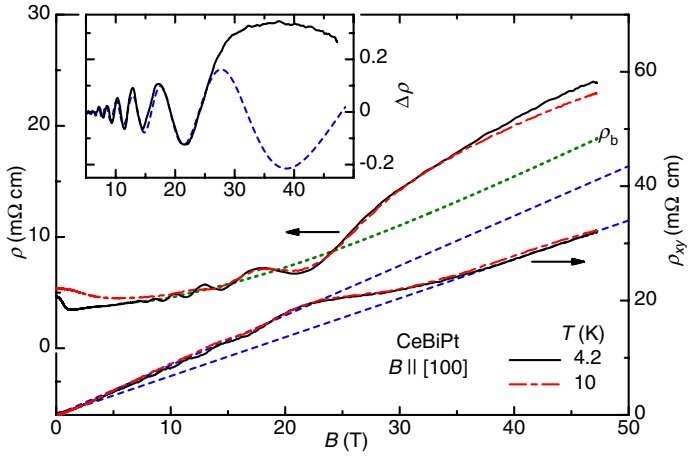

Figure 6. Field dependence of the longitudinal, ρ, and transverse, ρ_{xy}, resistivities of CeBiPt for different temperatures. The dashed lines are linear fits to the low- and high-field Hall data. The inset shows the SdH signal at 4.2 K after subtracting the steady background ρ_b from the pulsed-field ρ data. The dashed curve represents the behaviour expected theoretically.

(figure 4). The inset in figure 6 shows the expected SdH signal (dashed curve) in comparison to the experimental data (solid line). For the latter, it is necessary to estimate ρ_b, the steady background resistivity shown by the dotted line in the main frame of figure 6. Although there is some ambiguity in ρ_b, any reasonable estimate leads to the conclusion that the oscillating signal $\Delta\rho = (\rho - \rho_b)/\rho_b$ disappears above 25 T. For the theory curve (dashed line in the inset of figure 6), we used the standard SdH description [9] with the experimentally known parameters $F = 48$ T for the SdH frequency at 4.2 K, $m_c = 0.24\, m_e$ for the cyclotron mass and $T_D = 2.7$ K for the Dingle temperature. The good reproduction of the experimental data below 25 T indicates the field independence of m_c and T_D.

It is instructive to analyse the simultaneously measured Hall signal shown in figure 6 as well. The data clearly reveal a change of slope of the transverse resistance matching the field range where the SdH signal vanishes. In the present sample, this effect was found to be temperature independent between 1.8 and 10 K. The average Hall coefficient, $R_H = \rho_{xy}/B$, decreases by about 28% at highest fields (difference in the slopes of the two dashed lines in figure 6). In a simple one-band picture, the linear regression of the low-field ($B \lesssim 22$ T) Hall data results in a hole-like charge-carrier concentration of $n_h^{low} = (R_H e)^{-1} = 7.2(3) \times 10^{17}$ cm^{-3}, whereas at high fields ($B \gtrsim 38$ T) it increases to $n_h^{high} = 9.2(3) \times 10^{17}$ cm^{-3}.

Our data, therefore, show clear evidence for a field-induced change of the electronic band structure in the paramagnetic state of CeBiPt. The low-field data are in line with earlier [7] as well as more recent band-structure calculations (see below) [2]. The SdH results thereby correspond to a predicted hole-like Fermi surface. From the experimental side, a detailed analysis of the high-field Fermi-surface topology from our data is excluded due to the lack of any detectable SdH signal at these fields.

It was mentioned above that the temperature-dependent Fermi-surface change is absent for the homologous non-4f compound LaBiPt. Consequently, pulsed-field experiments were performed with both longitudinal and transverse components of the resistance being measured

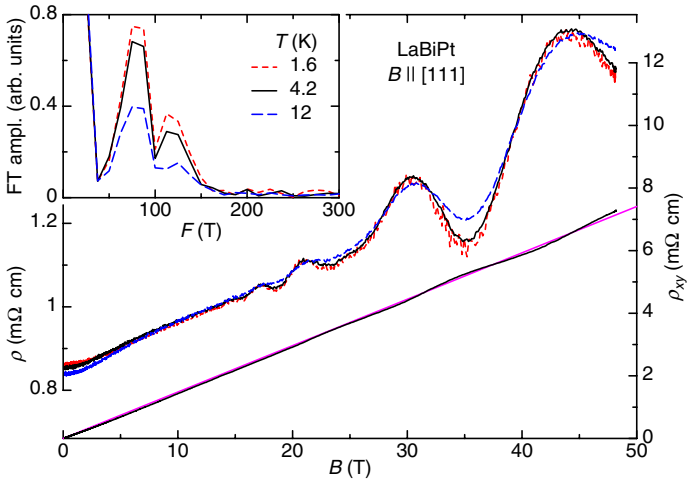

Figure 7. Field dependence of the longitudinal and transverse resistivities of LaBiPt for different temperatures. The dashed line is a linear fit to the Hall data. The inset shows the Fourier spectra of the longitudinal-resistivity data.

simultaneously. As shown in figure 7, for LaBiPt neither the longitudinal resistance nor the Hall effect reveal any deviation from a well-behaved metal. The SdH oscillations persist up to the highest fields with temperature-independent frequency and, most remarkably, the slope of the transverse signal remains—except for small SdH traces—constant yielding a field-independent Hall coefficient. Accordingly, in the single-band picture, the charge-carrier concentration in LaBiPt remains at $n_h = 4.2(2) \times 10^{18}\,\mathrm{cm}^{-3}$.

The Fourier transformation of the ρ data between 10 and 50 T (inset of figure 7) shows two peaks, one at about 80 T and the second at about 120 T. This is very well in line with the results from a relativistic band-structure calculation predicting two slightly different hole Fermi surfaces [6]. This leads to the beat pattern of the SdH signal directly visible in $\rho(B)$. The further predicted two sets of very small electron surfaces [6] cannot be resolved in the experiment. The effective cyclotron masses, extracted from the temperature dependence of the SdH-oscillation amplitudes, are $m_{c1} = 0.20(2)$ for the SdH orbit with 80 T frequency and $m_{c2} = 0.24(4)$ for the 120 T orbit. Again, this is in excellent agreement with the theoretical predictions [6].

From our experimental results, it is obvious that the Ce 4f moments play the major role in the temperature and field-dependent peculiarities observed in CeBiPt. Without 4f electrons, as in LaBiPt, the Fermi surface remains stable as expected for an ordinary metal. It was suggested that the temperature-dependent change of the Fermi surface in CeBiPt might be caused by a partial hybridization of the 4f electrons [7]. This was motivated by band-structure calculations which result in largely different Fermi surfaces for either localized or itinerant 4f electrons. A possible explanation for the observed features in large applied magnetic fields, therefore, would be that with increasing magnetic field, the f electrons become decoupled from the delocalized electrons. A field-dependent decrease of the 4f hybridization is well known from Ce-based heavy-fermion compounds, such as $CeCu_6$ and CeB_6 [11]. However, as noted already, in contrast to these materials the Kondo effect plays no significant role in CeBiPt.

In order to check the above scenario, the magnetization of CeBiPt was measured in pulsed fields [2]. If the f electrons would lose their itinerant character at high magnetic fields, one would

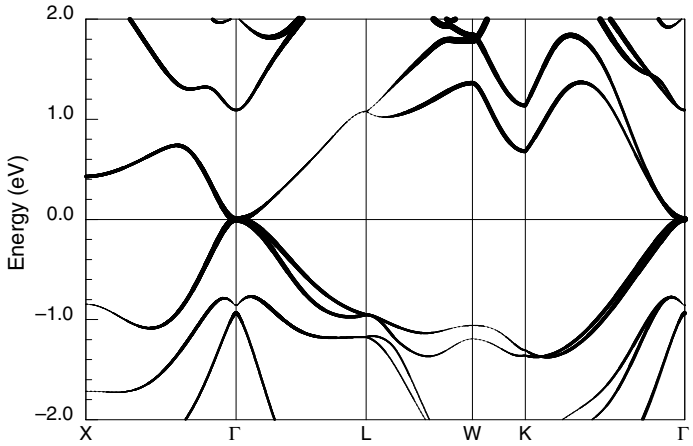

Figure 8. Band structure of nonmagnetic CeBiPt. The amount of Ce 5d character in the bands is indicated by the thickness of the lines.

expect a feature, i.e., some increase, in the magnetization at ∼25 T. There is, however, no sign of any unusual feature in the magnetization at 25 T [2]. We therefore exclude a field-induced decoupling of the f electrons from the itinerant charge carriers. Alternatively, we assume that the f electrons are localized already in the ground state, in line with the very small observed Sommerfeld coefficient of the specific heat. In this scenario, a field dependence of the band structure via exchange coupling with field-polarized 4f states may explain the measured anomalies.

3.3. Band-structure calculations

For *R*BiPt, realistic band structures can only be obtained when spin–orbit coupling is included, i.e., when relativistic band-structure calculations are performed. Only then are both LaBiPt and CeBiPt found to be semimetals, otherwise semiconducting behaviour results [6, 7]. In first calculations for CeBiPt, assuming localized 4f states, two small hole-like Fermi surfaces are found around Γ, with a cross-section similar to that measured [7]. The predicted very small electron-like pockets seem to be too small to be experimentally observable. When itinerant 4f electrons are assumed, the Fermi-surface topology changes completely, i.e., a complicated multi-connected Fermi-surface monster would result that is entirely at odds with experiment.

We later recalculated [2] the zero-field band structure of CeBiPt using a recent [12], high-precision four-component relativistic version of the full-potential local-orbital (FPLO) code [13]. The Perdew–Zunger parametrization of the exchange-correlation potential in the local spin-density approximation (LSDA) was used. A basis set of optimized local orbitals with 5s, 5p, 6s, 6p and 5d states for Ce, Bi and Pt, respectively, was used. The Ce 4f states were not included in the valence basis and localized by use of a confining potential. A spherically averaged 4f charge and spin density was assumed in this so-called open-core approach (surveyed in [14]). Self-consistent calculations were performed with 8000 k points in the full Brillouin zone and 2000 Fourier components per atom for the Ewald-potential representation. Up to two million k points in the full Brillouin zone were used for the precise calculation of the Fermi surface and band structure.

The resulting band-structure (figure 8) is very similar to that published earlier [7], but the semi-metallic character is yet more prominent with almost vanishing Fermi surfaces (see also

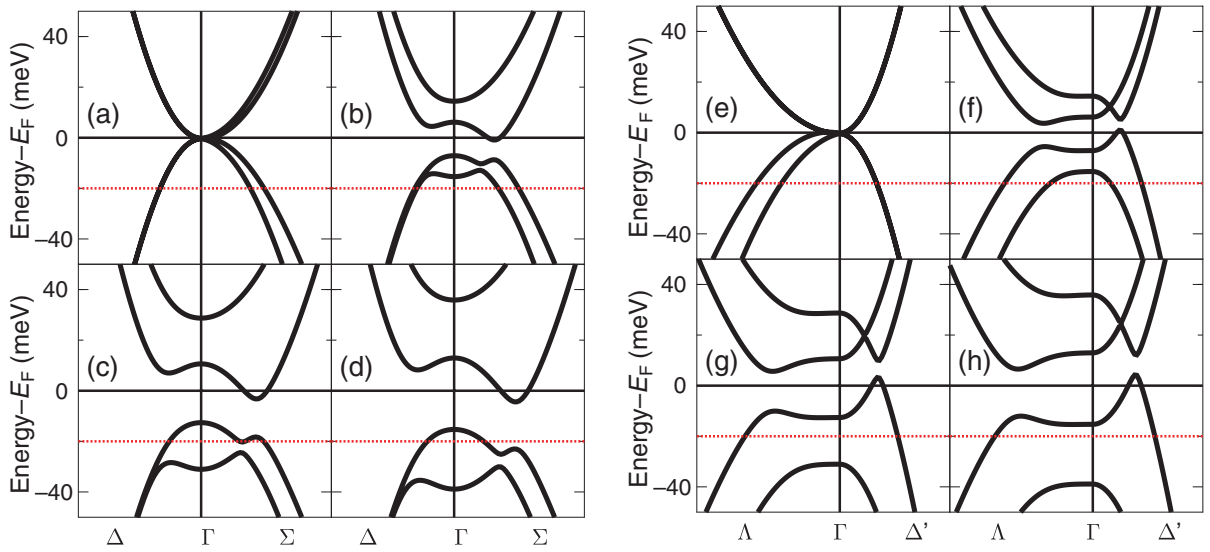

Figure 9. LSDA bands of CeBiPt close to the Brillouin-zone centre along the symmetry lines Δ (from (0.1 0 0) to (0 0 0) in units of $2\pi/a$) and Σ (from (0 0 0) to (0.075 0.075 0)) (left panel) and along Λ (from (0.075 0.075 0.075) to (0 0 0)) and Δ′ (from (0 0 0) to (0 0 0.1)) (right panel). The nominal E_F is at zero energy; the shifted Fermi level that yields the correct Fermi-surface area is indicated at −20 meV by the dotted line. Panels (a) and (e) show the nonmagnetic case with unpolarized 4f shell; in (b, f), (c, g) and (d, h) the 4f spin moment is fixed to be 0.4 μ_B, 0.8 μ_B and 1.0 μ_B, respectively. The combined effect of spin–orbit coupling and spin polarization reduces the symmetry from cubic (a, e) to tetragonal (b–d, f–h), where the lines from Γ to (0 0 1) and Γ to (1 0 0) are no longer equivalent.

the enlargement of the bands close to E_F in figure 9). The experimentally observed hole-pocket areas can be matched if the Fermi level is shifted by 20 meV to lower energy (indicated by the dotted line in figure 9). This shift corresponds to a tiny change of the valence-electron number, $\Delta N/N \approx 10^{-5}$. Such an uncertainty might be caused by a minute off-stoichiometry of the samples below the limit of detectability.

In the energy region shown, strongly hybridized Ce 5d, Bi 6p and Pt 5d orbitals with admixtures of Pt 6p and Ce 6p states form the bands. The amount of Ce 5d character in the bands is indicated by the thickness of the lines in figure 8. Close to E_F (±0.5 eV), the Ce 5d orbitals have the largest weight in the bands. Intra-atomic exchange splits the Ce 5d levels when the Ce 4f electron is polarized. Consequently, the bands close to the centre of the Brillouin zone which contribute to the Fermi surface are sensitive to a polarization of the Ce 4f electron in an external field.

This 4f polarization, induced by the applied external magnetic field, has been taken into account for the band-structure calculation by use of a partly spin-polarized 4f density in the open-core approach. The resulting exchange-split Ce-5d bands are shown in figures 9(b)–(d) and (f)–(h). The 4f spin polarization is gradually enhanced from compensated spin densities (figures 9(a) and (e)) to a field-saturated paramagnet, i.e., to a completely polarized 4f state (figures 9(d) and (h)). With increasing 4f polarization, the electronic bands are split correspondingly in a

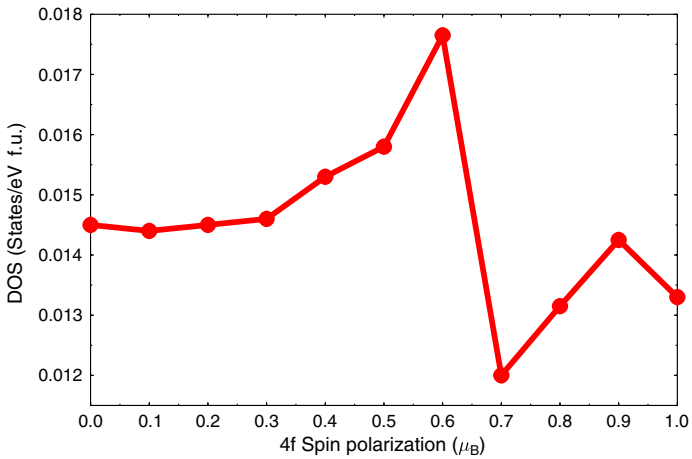

Figure 10. Density of states at the shifted Fermi level in dependence of the degree of 4f polarization.

Zeeman-like fashion into four equidistant levels. The lowest of the four levels crosses the Fermi level before the 4f moment is saturated. This is a transition from a two-band to a one-band situation which necessarily yields a change of the effective number of charge carriers. The second-lowest band has a characteristic minimum along the Σ line which crosses the shifted Fermi level for a 4f spin moment of about 0.8 μ_B, so that the corresponding extremal orbit of the Fermi surface separates into smaller sheets with frequencies $\lesssim$ 20 T which would explain the peculiarities of the SdH signal above 25 T.

Figure 10 shows the dependence of the DOS at the shifted Fermi level ($E_F - 20$ meV) on the degree of 4f polarization. At a polarization of about 0.6 μ_B, the lower of the two hole pockets vanishes, and a related van Hove singularity moves through the shifted Fermi level. The shape of this singularity is indicative of a strongly reduced dispersion close to the top of the band. This is in accordance with the flattening of the Zeeman-split bands at the Fermi energy with increasing exchange polarization (figure 9). The analysis shows that the anomalies can be classified as being caused by a magnetic-field-induced Lifshitz transition [1].

It lies in the very nature of such topological transitions that extreme care has to be taken concerning the resolution of small features in k-space. The calculations related to figure 10, therefore, were done with a fine sampling mesh of 128^3 k points in the Brillouin zone.

Within the above scenario, the field-induced band-structure modification should depend sensitively on the exact stoichiometry of the investigated samples, which determines the Fermi-level position. Furthermore, the 4f polarization should depend on the temperature. That is, at higher temperatures the Lifshitz transition should be shifted to higher magnetic fields. In earlier experiments [2] we only gathered data for temperatures below 10 K. Therefore, in order to test these assumptions additional pulsed-field measurements up to higher temperatures were performed on a second CeBiPt crystal out of the same batch as the previously measured one.

The main features of the longitudinal and transverse resistances for this second sample (figure 11) confirm the results presented above. In contrast to the earlier findings, however, only a very small temperature dependence of the SdH frequency is found as can be seen from the oscillating signal $\Delta\rho$ shown in the inset of figure 11. F reduces from about 54 T at 3.9 K to 50 T at 10 K. Compared to SdH frequencies of 46 and 35 T respectively, as measured for the other crystal,

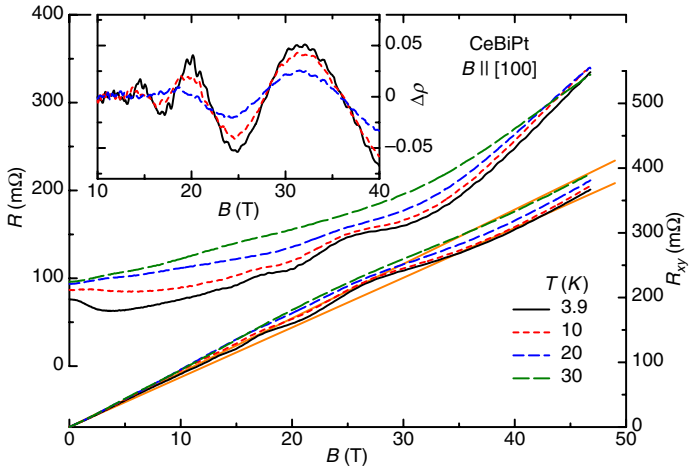

Figure 11. Field dependence of the longitudinal and transverse resistances of a second CeBiPt sample for different temperatures. The dotted lines are linear fits to the low- and high-field Hall data. The inset shows the SdH signal after subtracting a steady background from the pulsed-field data.

the relative change in F is much smaller and, even more remarkably, the Fermi-surface cross-section is considerably enlarged. This points to a stronger shift of the Fermi level in the second CeBiPt sample that might be related to a larger, but still small, off-stoichiometry. In line with this higher SdH frequency and a possible larger Fermi-level shift, the SdH oscillations persist to much higher magnetic fields and the slope change of the Hall signal is much smaller (only about 10% as visualized by the dotted lines in figure 11). Again, the magnetic field where the strong increase of the longitudinal resistance occurs (at about 35 T for $T = 3.9$ K), coincides with the decrease of R_H. In accordance with expectation, this transition moves to higher magnetic fields at higher temperatures and the Hall signal becomes more and more linear with field (figure 11). It is, however, fair to say that for the second sample somewhat higher magnetic fields would be necessary to verify the transition unambiguously.

4. Conclusion

We presented neutron-scattering data on CeBiPt that revealed a simple commensurable antiferromagnetic structure below the Néel temperature of 1.15 K. Strong localized magnetic Ce moments are detected, although part of the expected moment for a Γ_8 ground state is missing. Electrical-transport measurements in the paramagnetic state show a remarkable field-induced modification of the electronic band-structure in CeBiPt. Above a certain threshold field the SdH signal disappears and the Hall coefficient changes clearly. These effects are found to be sample and temperature dependent. The absence of any unusual behaviour in electrical-transport data for the non-4f compound LaBiPt proves the relevance of the magnetic 4f states for the observed features. Relativistic band-structure calculations taking into account the spin polarization of the 4f states can very well explain the experimental results and indicate that the realized band-structure change can be classified as a magnetic-field-induced Lifshitz transition.

Acknowledgments

The work at Dresden was supported by the DFG through SFB 463 and the BMBF (FKZ 035C5 DRE). The work at Karlsruhe was supported by the DFG through SFB 195. The work at Hiroshima was supported by the COE Research (13E2002) in a grant-in-aid from the Ministry of Education, Culture, Sports, Science and Technology of Japan.

References

[1] Lifshitz I M 1969 *Zh. Eksp. Teor. Fiz.* **38** 1569
[2] Kozlova N *et al* 2005 *Phys. Rev. Lett.* **95** 086403
[3] Canfield P C, Thompson J D, Beyermann W P, Lacerda A, Hundley M F, Peterson E, Fisk Z and Ott H R 1991 *J. Appl. Phys.* **70** 5800
[4] Fisk Z *et al* 1991 *Phys. Rev. Lett.* **67** 3310
[5] Robinson R A, Purwanto A, Kohgi M, Canfield P C, Kamiyama T, Ishigaki T, Lynn J W, Erwin R, Peterson E and Movshovich R 1994 *Phys. Rev.* B **50** 9595
[6] Oguchi T 2001 *Phys. Rev.* B **63** 125115
[7] Goll G, Hagel J, Löhneysen H v, Pietrus T, Wanka S, Wosnitza J, Zwicknagl G, Yoshino T and Takabatake T 2002 *Europhys. Lett.* **57** 233
[8] Pietrus T, Miokovi ć T, Schröder A, Löhneysen H v, Yoshino T, Takagi K, Umeo K and Takabatake T 2000 *Physica* B **281–282** 745
[9] Shoenberg D 1984 *Magnetic Oscillations in Metals* (Cambridge: Cambridge University Press)
[10] Wosnitza J, Hagel J, Kozlova N, Eckert D, Müller K-H, Mielke C H, Goll G, Yoshino T and Takabatake T 2004 *Physica* B **346–347** 127
[11] Fisk Z and Thompson J D 1992 *Physical Phenomena at High Magnetic Fields* ed E Manousakis, P Schlottman, P Kumar, K S Bedell and F M Müller (Redwood City, CA: Addison-Wesley) p 197 and references therein
[12] Opahle I 2001 *PhD Thesis* Technische Universität Dresden
Eschrig H, Richter M and Opahle I 2004 *Relativistic Electronic Structure Theory—Part II: Applications* ed P Schwerdtfeger (Amsterdam: Elsevier) p 723
[13] Koepernik K and Eschrig H 1999 *Phys. Rev.* B **59** 1743; online at http: //www.FPLO.de
[14] Richter M 1998 *J. Phys. D: Appl. Phys.* **31** 1017